Semiconductor−Metal Nanocomposites. Photoinduced Fusion and Photocatalysis of Gold-Capped TiO_2 (TiO_2/Gold) Nanoparticles

Amy Dawson[†] and Prashant V. Kamat*

Notre Dame Radiation Laboratory, Notre Dame, Indiana 46556-0579

Received: September 16, 2000

Semiconductor/metal composite nanoparticles have been synthesized by chemically reducing $HAuCl_4$ on the surface of preformed TiO_2 nanoparticles. These gold-capped TiO_2 nanoparticles (particle diameter 10−40 nm) were stable in acidic (pH 2−4) aqueous solutions. At low [TiO_2]:[Au] ratio (<1:1), these composite nanoparticles are bigger in size (20−40 nm) and readily undergo aggregation. The TiO_2/Au nanoparticles with TiO_2:Au ratio ≥1:10 were relatively stable to 532 nm laser irradiation. On the other hand 532 nm laser pulse excitation of aggregated nanoparticles ([TiO_2]:[Au] ≤ 1:1) led to morphological changes as they fused to produce large-size particles. Laser-induced melting/fusion was confirmed from the growth in the particle size as well as the disappearance of the aggregation absorption band. The process of melting and fusion occurred with an apparent rate constant of 1.25×10^9 s^{-1}. The role of the gold layer in promoting the photocatalytic charge transfer has been probed using thiocyanate oxidation at the semiconductor interface. More than 40% enhancement in the oxidation efficiency is seen with TiO_2/Au nanoparticles capped with low concentration of the noble metal.

Introduction

The emerging field of semiconductor and metal nanoparticles has stimulated much interest in recent years because of their size and shape dependent electronic properties.[1−5] The functional properties of such materials can be greatly improved by capping the semiconductor or metal nanocluster with another layer of compatible material. Such core/shell geometry not only improves the stability of the nanoparticles but also expands the scope of composite nanoclusters in a wide array of applications (e.g., luminescent displays, microelectronics photochemical solar cells, sensors and memory devices).[6−8] Some examples of core/shell type nanomaterials include semiconductor/semiconductor,[9−13] semiconductor/metal,[14] metal/semiconductor,[15−17] metal/metal,[18−21] and metal/metal oxide[22−25] systems.

One of the major goals behind designing composite nanoparticles is to improve the catalytic properties or to tune the luminescent or sensing properties (Scheme 1). For example single component semiconductor nanoparticles exhibit relatively poor photocatalytic efficiency (<5%) since the majority of the photogenerated charge carriers undergo recombination.[26] Semiconductor/semiconductor or semiconductor/metal composite nanoparticles facilitate charge rectification in these systems. The deposition of a noble metal on semiconductor nanoparticles is an essential factor for maximizing the efficiency of photocatalytic reactions.[27,28] The noble metal (e.g., Pt), which acts as a sink for photoinduced charge carriers, promotes interfacial charge-transfer processes. A direct correlation between the work function of the metal and the photocatalytic activity for the generation of NH_3 from azide ions has been made for metallized TiO_2 systems.[29] Composite semiconductor systems have also been shown to improve the photoconversion efficiency of dye-sensitized photochemical solar cells[30,31] and photocatalytic reactions.[32,33]

SCHEME 1: Interfacial Charge Transfer Processes in a Metal−Semiconductor Nanoparticle

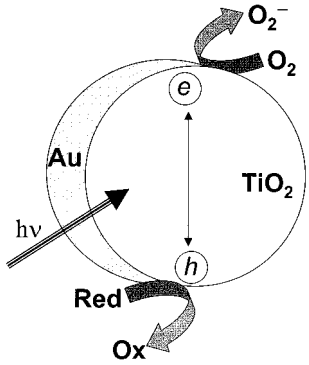

Despite several efforts to synthesize semiconductor/metal composite nanoparticles,[16,34−36] little information is available on the photodynamics of these materials. In our earlier study with Au/CdS, we probed the electron transfer between photoexcited CdS layer and gold core using picosecond laser flash photolysis.[15] Similarly gold nanoparticles deposited on nanostructured TiO_2 films have been shown to enhance the photocurrent generation efficiency by a factor of 3.[37] Recently, Halas and co-workers[38−41] have investigated the effect of an oxide core on the optical properties of gold nanoshell and chemically bound gold nanoparticles. Fundamental understanding of the photoinduced interactions between a semiconductor and metal as well as the interfacial charge-transfer process in nanocomposites is important to elucidate the role of noble metals in semiconductor assisted photocatalysis. In this report we describe a simple methodology for preparing gold-capped TiO_2 nanoparticles in aqueous medium and the morphological changes associated with visible laser excitation. Laser flash photolysis experiments that elucidate the ability of TiO_2/Au nanoparticles

* Address correspondence to this author. Email: pkamat@nd.edu or http://www.nd.edu/~pkamat.

[†] Undergraduate Coop Program, University of Waterloo, Canada.

10.1021/jp0033263 CCC: $20.00
Published on Web 01/04/2001

SCHEME 2: Adsorption and Reduction of $[AuCl_4]^-$ Ions on the TiO_2 Nanoparticle

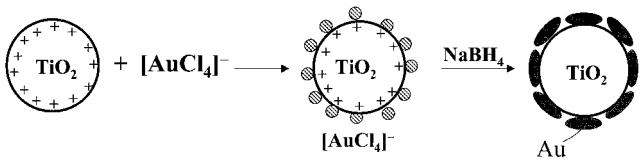

in promoting the photocatalytic oxidation of thiocyanate ions are also described.

Experimental Section

Preparation of TiO_2 Colloidal Suspension (5 mM). TiO_2 nanoparticles (particle diameter 5−10 nm) were prepared by dropwise addition of 2.97 mL of 10% titanium isopropoxide (Aldrich, 99.999%) in 1-propanol to 200 mL of deionized water with vigorous stirring. Prior to addition of titanium isopropoxide the pH of the water was adjusted to ∼1.5, with $HClO_4$. The solution was kept stirring in a stoppered glass flask. Freshly prepared colloidal suspension was used in all the experiments.

Preparation of TiO_2/Au Nanoparticles. Four different suspensions of gold-capped TiO_2 nanoparticles were prepared by keeping the gold concentration constant at 0.2 mM while varying the TiO_2 concentration from 4 to 0.05 mM. These four TiO_2/Au suspensions contained $[TiO_2]$:[Au] ratios of 20:1, 10:1, 1:1, and 0.25:1. (All the concentrations are based on molecular concentrations.) Scheme 2 shows the principle of preparation of the TiO_2/Au nanoparticles.

TiO_2/Au nanoparticles were prepared by adding the desired amount of 5 mM stock $HAuCl_4$ (Aldrich) solution to the colloidal TiO_2 suspension in water while stirring vigorously. The negatively charged $[AuCl_4]^-$ adsorbs strongly on the positively charged surface of the TiO_2 nanoparticles. The solution was stirred for an additional 5 min to allow complete adsorption of $[AuCl_4]^-$ ions onto the TiO_2 surface. Reduction of the $[AuCl_4]^-$ was achieved by the dropwise addition of sodium borohydride (8−10 mM for 20:1 and 10:1 ratios and 1 mM for 1:1 and 0.25:1 ratios) until a color change was observed. The reduced gold solutions made with TiO_2:Au ratios of 20:1, 10:1, and 1:1 were wine red in color, while the solution with a TiO_2:Au ratio of 0.25:1 solution was dark purple in color. All solutions used were freshly prepared and kept stirring in a closed flask until used.

Spectral and Particle Characterization. Solutions were transferred to a 1 cm quartz cuvette with a rubber septum and were deaerated for 15 min by bubbling N_2 gas prior to analysis. Absorption spectra were recorded using a Shimadzu 3101 PC spectrophotometer. All experiments were carried out at room temperature (296 K).

Transmission electron microscope (TEM) images were taken using a Hitachi H600 transmission electron microscope at a magnification factor of 200000×. One drop of sample was placed on a carbon-coated copper grid for imaging and blotted to remove excess liquid.

Picosecond laser flash photolysis experiments were performed with a 532 nm laser pulse from a mode-locked, Q-switched Continuum YG-501 DP Nd:YAG laser system (output 2−3 mJ/pulse, pulse width 18 ps). The white continuum picosecond probe pulse was generated by passing the fundamental output through a D_2O/H_2O solution.[42] Sample was transferred to a 1 cm quartz cuvette and degassed with N_2 for 15 min prior to photolysis and then continuously throughout photolysis. During photolysis, sample was flowed through the cell.

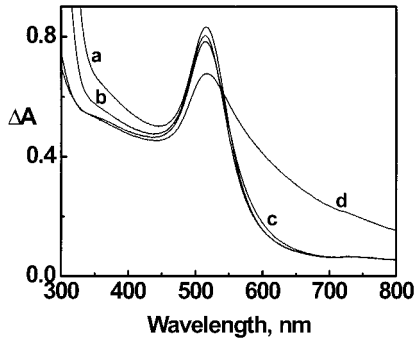

Figure 1. Absorbance spectra of Au/TiO_2 nanoparticles in water (pH ∼ 1.5). The gold concentration in these samples was 0.2 mM and the concentration of TiO_2 core was varied. The ratios of TiO_2:Au were (a) 20:1, (b)10:1, (c) 1:1, and (d) 0.25:1.

Results and Discussion

Absorbance Characteristics of TiO_2/Au Particles. Metijevic and co-workers have shown that a variety of surface coatings can be produced on cores of very different compositions.[25,43,44] They have shown that the formation of coatings on particles dispersed in liquids need not depend on specific interfacial reactions. Averitt et al.[45] have deposited a gold nanoshell onto silica nanoparticles by mixing amine-functionalized silica particles with a solution of gold nanoparticles for directly attaching gold nanoparticles to the silica surface.

The gold-capped TiO_2 nanoparticles in the present experiments were prepared by first synthesizing TiO_2 suspension in water (stabilized at pH 1.5) and then capping these particles with gold nanocrystallites. The positively charged TiO_2 core acts as a support to adsorb $[AuCl_4]^-$ ions that are subsequently reduced by $NaBH_4$. Lack of binding groups in our experiments will result in a loosely bound layer of gold nanocrystallites on the TiO_2 core. It is likely that the gold capping formed on the TiO_2 nanoparticles is a discontinuous shell made up of several small gold nanoclusters or islands. We varied the $[TiO_2]$:[Au] ratio by keeping the $[AuCl_4]^-$ concentration constant and varying the concentration of TiO_2. Figure 1 shows the ground-state absorbance spectra of the four different TiO_2/Au colloidal solutions in aqueous solution. All the four solutions contained the constant amount of gold (0.2 mM), but different TiO_2 core concentrations. These experimental conditions allowed us to achieve different gold distribution on the TiO_2 core and compare the spectral properties.

In the solutions containing higher TiO_2 concentrations (i.e., when the ratio of TiO_2:Au is maintained at a ratio greater than 1:1), a sharp and prominent absorption corresponding to the surface plasmon band of gold is observed. The stability of these suspensions was quite good and they were stable overnight. At lower TiO_2 concentrations (i.e., when the ratio of TiO_2:Au is maintained at 0.25:1), we observe a significant dampening of the surface plasmon band with simultaneous appearance of an aggregation band in the red-IR region (spectrum d). The lack of available charged TiO_2 surface at low TiO_2 concentrations renders the TiO_2/Au nanoparticles unstable, thus inducing some aggregation. Conversely, stable sols of TiO_2/Au can be prepared by simply increasing the concentration of the TiO_2 core. It should be noted that the gold reduction carried out in the absence of TiO_2 nanoparticles using the same experimental procedure did not yield stable nanoparticles.

It has been shown that the presence of a dielectric core can induce dipolar plasmon resonances in the infrared.[39,40] The optical absorption of a thin film consisting of silica core/gold shell nanostructures can be varied from 800 to 2200 nm by

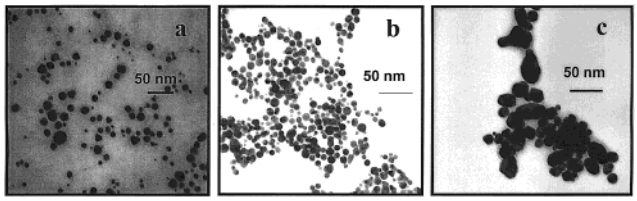

Figure 2. TEM images of TiO_2/Au nanoparticles. The ratios of TiO_2:Au were (a) 20:1, (b) 1:1, and (c) 0.25:1.

varying the relative size of the core and shell. However, no such infrared absorption could be seen for the silica core/gold nanoshell[45] or gold core/silica nanoshell[23,24] particles suspended in aqueous medium. The spectral features of SiO_2/Al_2O_3/Au shown in Figure 1B do not indicate any significant red shift in the plasmon absorption or absorption bands in the infrared, thus ruling out direct interaction with the SiO_2/Al_2O_3 surface. Weak interaction between the SiO_2/Al_2O_3 and the gold layer and the dominance of surrounding aqueous medium are the possible reasons for not observing the influence of dielectric oxide core.

Transmission Electron Microscopy (TEM). Transmission electron micrographs of three different TiO_2/Au composite nanoparticles are shown in Figure 2. For the high core:shell (TiO_2:Au) ratio of 20:1 (as well as for 10:1) we observe fairly well dispersed particles with a particle diameter of ~10 nm. These particles have a relatively thin gold shell with no significant change in particle size compared to the TiO_2 core. For a TiO_2:Au ratio of 1:1, we observe an increase in the size of TiO_2/Au particles (particle diameter 10−20 nm). These particles also tend to be in close proximity to each other. As observed from the absorption spectrum in Figure 1, these particles maintain individual identity and do not exhibit noticeable aggregation effects. However the TiO_2/Au particles containing a low concentration of TiO_2 (TiO_2:Au ratio of 0.25:1) showed significant growth in the particle size with a particle diameter ranging from 20 to 40 nm. Moreover, these particles remain closely packed, thus inducing aggregation effects. As can be seen from spectrum d in Figure 1, these close-packed clusters exhibit absorption in the red and infrared region. These observations support the hypothesis that the gold capping continues to occur on TiO_2 particles even at very low ratio of TiO_2:Au. The decreased TiO_2 core concentration leads to the formation of larger size particles with decreased stability of the sol.

Laser-Induced Morphological Changes. As shown in recent studies, gold nanoparticles and nanorods can undergo either fusion or fragmentation during visible laser irradiation.[46−49] Both the duration and intensity of the laser pulse control the type of morphological changes that occur during the laser irradiation. To see whether gold-capped TiO_2 nanoparticles are also susceptible to melting under laser irradiation, we monitored the morphological changes by means of TEM images and spectral changes.

Figure 3 shows the TEM images recorded after 5 min laser irradiation of an aqueous suspension of TiO_2/Au nanoparticles at different core:shell ratios. (Please refer to Figure 2 for the shape and size of particles before laser irradiation.) The TiO_2/Au samples containing a high TiO_2:Au ratio (>1:1) exhibited remarkable stability toward laser irradiation. The TEM images did not show any major changes in the particle size or shape. Formation of a few small nanoparticles may be indicative of a photofragmentation process but occurred only to a limited extent. The TiO_2/Au particles of TiO_2:Au ratio of 1:1 showed the presence of few large-size particles. However, the formation of very large size particles was clearly evident in the case of TiO_2/

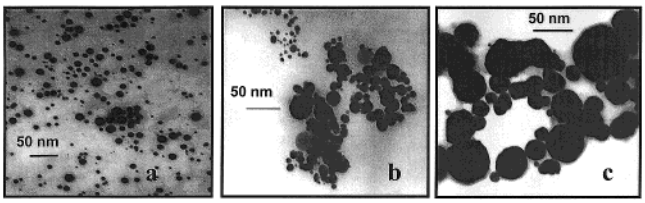

Figure 3. TEM images of TiO_2/Au nanoparticles recorded after exciting the samples with 532 nm laser pulses (10 Hz, 3 mJ/pulse) for 5 min. The ratios of TiO_2:Au were (a) 20:1, (b) 1:1, and (c) 0.25:1. A growth in particle size can be seen in (b) and (c) when compared to the same samples before photolysis in Figure 2.

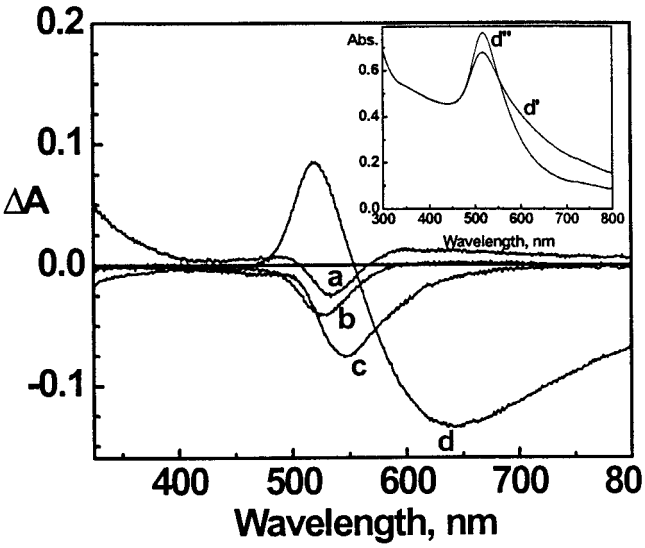

Figure 4. Changes in the absorption spectra of photolyzed TiO_2/Au nanoparticles. The absorption spectra were recorded after 5 min of laser pulse excitation (corresponding samples prior to photolysis were used as reference). The difference absorption spectra correspond to the TiO_2:Au ratios of (a) 20:1, (b) 10:1, (c) 1:1, and (d) 0.25:1. The inset shows the absorption spectra of TiO_2/Au nanoparticle (TiO_2:Au ratio of 0.25:1) suspension before (d′) and after (d″) laser photolysis using water as reference.

Au particles with a TiO_2:Au ratio of 0.25:1. The particles grew from 20−40 to 50−100 nm in diameter. An increase in the volume of 6−8 times suggests that several gold-capped TiO_2 nanoparticles that are in immediate contact with each other must be undergoing a fusion during the 532 nm laser pulse excitation.

As shown in our earlier laser irradiation studies of the thionicotinamide-capped Au nanoparticles, the aggregated clusters are extremely susceptible to laser-induced melting and fusion processes.[47] Since gold is the only species that absorbs at 532 nm, the incident laser excitation is usually localized in the gold layer of TiO_2/Au nanoparticles. As the gold particles are repeatedly bombarded with the laser pulse, the temperature of these particles increases and causes melting of these particles. Theoretical calculations have predicted a rise in temperatures up to 2500 K during laser excitation.[48] If these particles exist in the form of aggregates, the melting cluster assembly can fuse to form large-size particles. In the case of a larger TiO_2 core concentration, the TiO_2/Au particles are well separated from each other, thus facilitating the heat dissipation from the particles to the surrounding aqueous medium.

Laser-induced changes in TiO_2/Au nanoparticles were also monitored by recording changes in the absorption spectra for four different samples containing different core:shell ratios. Figure 4 shows the difference absorption spectra of the TiO_2/Au solutions recorded before and after 532 nm laser irradiation. (The spectra were recorded by keeping the irradiated solution

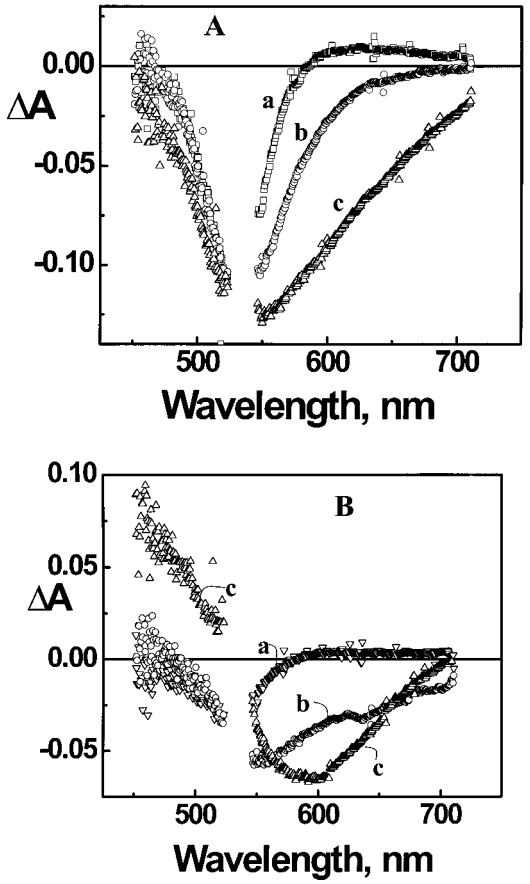

Figure 5. Transient absorption spectra recorded at (A) 150 ps and (B) 2000 ps after 532 nm laser pulse excitation of TiO_2/Au nanoparticles. The ratio of TiO_2:Au were (a) 10:1, (b) 1:1, and (c) 0.25:1 [TiO_2]:[Au] nanoparticles.

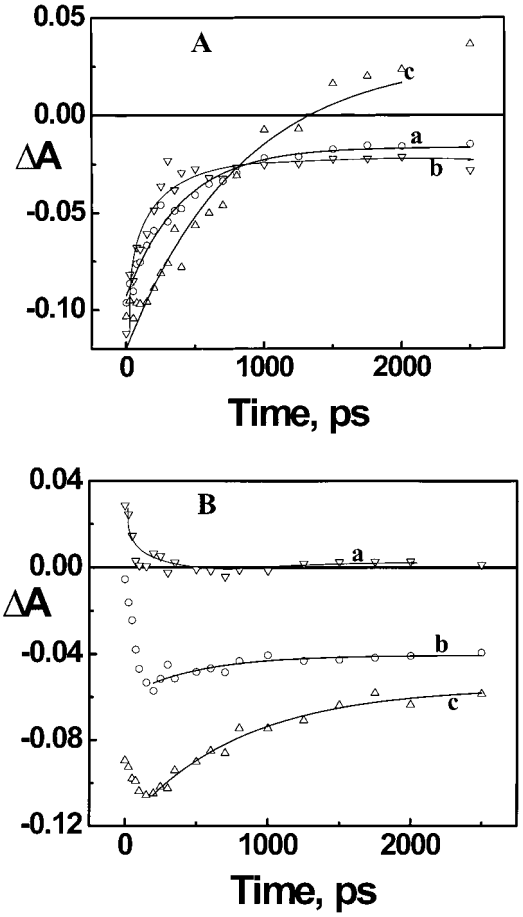

Figure 6. Absorption−time profiles recorded at (A) 510 and (B) 590 nm following laser (532 nm) photolysis of TiO_2/Au nanoparticles. The ratio of TiO_2:Au were (a) 10:1, (b) 1:1, and (c) 0.25:1 [TiO_2]:[Au] nanoparticles.

in the sample compartment and the solution prior to photolysis in the reference compartment of the spectrophotometer.) For samples with TiO_2:Au ratios of 20:1 and 10:1, the changes in the absorbance were relatively small. Only a small disappearance ($A < 0.03$) of the surface plasmon band was seen following the 5 min laser irradiation (532 nm excitation). Photoinduced fragmentation or dissolution of the gold layer can contribute to the small decrease in the surface plasmon band. For 1:1 TiO_2/Au nanoparticles the bleaching in the plasmon band was larger, suggesting that laser irradiation has a significant impact on the nanoparticles containing lower TiO_2 concentrations.

A more pronounced absorption change was seen when the TiO_2/Au nanoparticles with a ratio of 0.25:1 were subjected to laser irradiation. The difference absorption spectrum shows two distinct spectral features, viz., a bleaching in the 550−800 nm region and a growth of absorbance in the 500−550 nm region. Unlike the three previous spectra (spectra a−c in Figure 4) the spectrum does not show any bleaching at 532 nm, instead an increase in the surface plasmon band with a simultaneous disappearance of the aggregation band. These observations indicate that the TiO_2/Au nanoparticles become isolated as the aggregates disappear following the laser pulse irradiation. The inset in Figure 4 shows a narrowing of the plasmon band at 530 nm as the colloidal TiO_2/Au suspension is subjected to 532 nm laser photolysis.

The decrease in the absorbance seen in the 550−800 nm range indicates the disappearance of aggregates. As the clustered assembly of TiO_2/Au nanoparticles transform into bigger particles we observe the disappearance of the aggregation effect. Since these particles now behave as individual particles the aggregation effects cease to exist and we see an increase in the plasmon absorption band in the 530 nm region.

Picosecond Laser Flash Photolysis. We employed picosecond transient absorption spectroscopy to probe the photoinduced processes that lead to the morphological changes in the TiO_2/Au colloidal solutions. The colloidal suspensions at different core TiO_2 concentrations were subjected to 532 nm laser excitation, and difference absorbance spectra were recorded at different delay times. The representative transient spectra recorded at 150 and 2000 ps following the laser pulse excitation are shown in Figure 5A,B, respectively. The difference absorbance spectra recorded at 150 ps show a transient bleaching at 530 nm, which is characteristic of a bleaching of the ground-state absorption. As demonstrated earlier,[15,50,51] this bleaching arises from the excitation of electrons in the conduction band of a gold layer by the 532 nm laser pulse. These excited electrons no longer oscillate at the same frequency as the unexcited electrons, resulting in an overall decrease in the intensity of the plasmon band.

A significantly different transient absorption behavior is seen for the TiO_2/Au nanoparticles recorded at longer times (2 ns). The spectra recorded with a higher TiO_2:Au ratio ($\geq$1:1) show a decreased bleaching in the 530 nm region as the surface plasmon band of the gold shell recovers. The absorption−time profiles recorded at 510 and 590 nm show the recovery kinetics (Figure 6A,B, respectively) of the surface plasmon band. The fast component of the bleaching recovery corresponds to the relaxation of "hot" electrons via electron−phonon coupling and phonon−phonon relaxation of the lattice, respectively. For

pristine Au nanoparticles these fast and slow plasmon recovery processes occur with a lifetime of 2.5 and 50 ps, respectively.[51] Because of the longer laser pulse (pulse width 18 ps) we were not able to resolve the fast recovery component. It is evident that most of the long-term bleaching recovery is completed within the period of 500 ps. This behavior is similar to that exhibited by pristine Au nanoparticles in aqueous solutions. The residual bleaching observed at longer times essentially represents the fraction of the gold layer undergoing irreversible changes, possibly fragmentation or photodissolution. The fraction undergoing these changes is relatively small for higher TiO_2:Au ratios. Hence, we can conclude that the inner core of TiO_2 does not have significant influence on the photodynamics of the outer gold shell in the TiO_2/Au nanoparticles.

The TiO_2/Au suspension with a low TiO_2:Au ratio of 0.25:1, however, showed significantly different spectral behavior at longer times as the morphological changes dominated over the usual recovery of the surface plasmon band (spectrum d in Figure 5B). The bleaching maximum is shifted toward the red region (590 nm). As can be seen from the absorption time profile at 590 nm (Figure 6B), the bleaching is irreversible as the aggregate absorption disappears. The bigger and well-separated larger particles formed during the laser pulse excitation make the aggregation effect less probable and exhibit surface plasmon absorption properties similar to that of individual gold particles.

The disappearance of the aggregation band at 590 nm occurs with a lifetime of 0.8 ns. As indicated in the previous section the disappearance of the aggregation band parallels the growth of the plasmon absorption band. Thus, from the traces in Figure 6 we can infer that the complete morphological change of TiO_2/Au nanoparticles occurs with an apparent rate constant of 1.25×10^9 s^{-1}. A recent study of melting of gold nanorods has indicated that the melting process is completed within 35 ps.[52] In our study the longer lifetime of 0.8 ns represents the time scale required for complete morphological changes in TiO_2/Au core/shell aggregates following the laser pulse excitation.

The dependence of photofusion of TiO_2/Au nanoparticles on the laser intensity was also monitored. Since, the increased absorbance at 510 nm represents the formation of a fused TiO_2/Au nanoparticle, we can monitor the dependence of increased absorbance at 510 nm on the incident light intensity. The linear dependence of maximum absorbance at 510 nm versus $(\text{Intensity})^2$ shows that two or more photons (532 nm) are required to induce the photofusion process in these nanoparticles.

An alternate explanation for the formation of large-size particles following the laser irradiation of composite nanoparticles with lower TiO_2:Au ratio (0.25:1) would be to induce photofragmentation first and form extremely small size particles. These small particles would then aggregate in solution to form large-size particles. Although such a process might be prevailing, we do not consider it to be significant in the present experiments. If the photofragmentation/aggregation processes were to dominate, we would have expected a laser pulse limited bleach of the aggregation band, followed by a slower diffusion limited aggregation process to form large-size nanoparticles. The transient bleaching observed at 590 nm (Figure 6), which match well with the transient absorption growth at 510 nm (time constant of 0.8 ns) does not support the argument of sequential processes. In other words, these two processes, viz., disappearance of aggregation and appearance of plasmon absorption, occur simultaneously following the laser pulse excitation. Moreover, we do not observe a transient absorption growth (or decay) on a longer time scale that can be attributed to the slow diffusion-limited particle growth process. It is also important to note that we do not see formation of large-size particles in the case of composite nanoparticles that contain a higher TiO_2:Au ratio ($\geq$1:1). The probability of fusion in this case is small since these particles are well dispersed in the solution. As confirmed in two other examples, the presence of close-packed aggregates is a prerequisite for inducing photofusion and forming large-size particles. In these two independent experiments we formed gold nanoparticle aggregates via thiol addition or binding with a cationic dye to the gold nanoparticles. Short-term laser irradiation produced large particles while extended laser irradiation further fragmented large-size particles into very small particles.

It is evident from both transient absorption and steady-state spectra that the TiO_2/Au nanoparticles having larger TiO_2:Au ratios show better stability toward laser irradiation. The clustering of aggregates observed at low TiO_2:Au ratio facilitates dramatic morphological changes as they melt and fuse to form larger composite nanoclusters. While previous studies have focused on single component metal nanoparticles or nanorods, the present study highlights melting/fusion of a gold and TiO_2 composite. The schematic diagram shown in Figure 7 shows a possible pathway leading to the formation of multiple core nanocomposites. While the laser-induced fusion is a unique way to synthesize multicore/shell composite nanoparticles, direct applications of these systems remains to be explored.

Application of TiO_2/Au Nanoparticles in Photocatalysis. One of the major applications of metal/semiconductor composite system is in the area of photocatalysis. It has been shown that the photocatalytic electron transfer processes at the semiconductor interface can be greatly enhanced by depositing a noble metal on the semiconductor particle.[34,53−56] As shown previously, TiO_2 nanoparticles undergo charge separation under band gap excitation (e.g. = 3.2 eV). The 337 nm laser pulse is therefore capable of exciting TiO_2 nanoparticles and initiating the redox reactions at the interface. The photogenerated holes are capable of oxidizing thiocyanate ions at the semiconductor interface.[57] The thiocyanate radicals ($(SCN)_2^{\bullet -}$) generated in the photocatalytic oxidation can be conveniently monitored from its absorbance at 480 nm.[57,58]

The transient absorption spectra recorded following 337 nm laser pulse excitation of TiO_2 nanoparticles and TiO_2/Au nanoparticles containing 25 mM NaSCN are shown in Figure 8A,B, respectively. The spectra a in both sets of experiments show an absorption maximum corresponding to the formation of $(SCN)_2^{\bullet -}$ radicals (reactions 1−4). In the case of TiO_2

$$(TiO_2)Au + h\nu \rightarrow (TiO_2(e + h))Au \quad (1)$$

$$(TiO_2(e))Au + O_2 \rightarrow (TiO_2)Au + O_2^- \quad (2)$$

$$TiO_2(h) + SCN- \rightarrow (TiO_2)Au + SCN^{\bullet} \quad (3)$$

$$SCN^{\bullet} + SCN^- \rightarrow (SCN)_2^{\bullet -} \quad (4)$$

nanoparticles (Figure 8A) the thiocyanate radicals decay as they undergo irreversible chemical changes and/or recombination with conduction band electrons. In the case of TiO_2/Au nanoparticles, a new band appears at 390 nm as the transient absorption corresponding to $(SCN)_2^{\bullet -}$ decayed. As confirmed in our pulse radiolysis experiments,[59] the 390 nm absorption

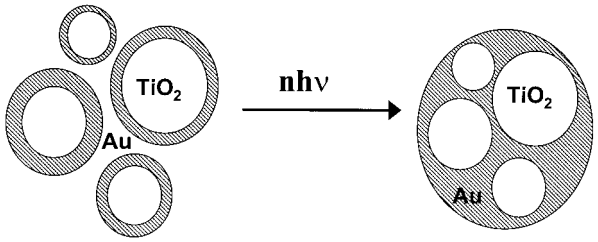

Figure 7. Schematic diagram illustrating the fusion of TiO_2/Au nanoparticles.

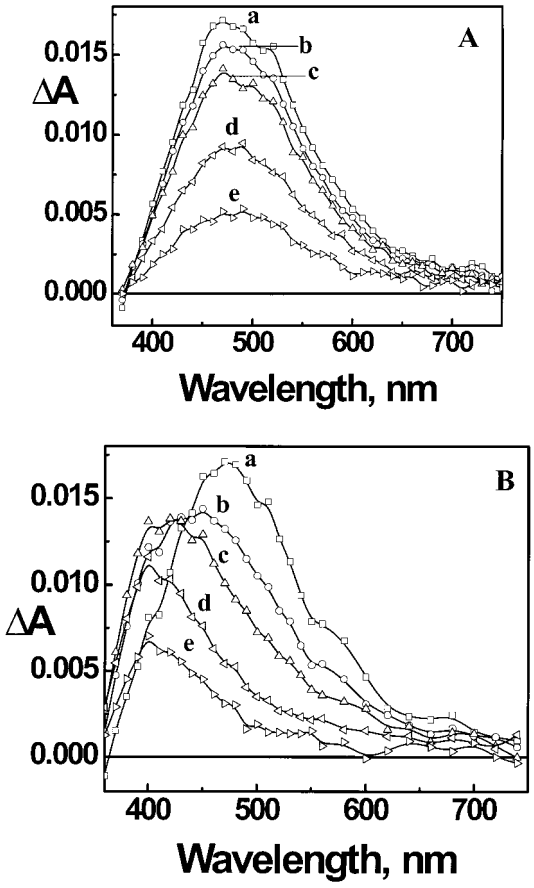

Figure 8. Transient absorption spectra recorded at (a) 0.5 μs, (b) 5 μs, (c) 10 μs, (d) 30 μs, and (e) 70 μs after following 337 nm laser excitation of (A) TiO_2 (12 mM) and (B) TiO_2/Au (12 mM TiO_2 and 0.013 mM Au) colloidal suspension containing 25 mM NaSCN in aqueous solution.

band represents complexation between $(SCN)_2^{\bullet-}$ radicals and the gold surface.

$$(TiO_2)Au + (SCN)_2^{-\bullet} \rightarrow [(TiO_2)Au...(SCN)_2^{-\bullet}] \quad (5)$$

This complex eventually decays (lifetime ~100 μs) by oxidizing the gold surface. The extent with which the photogenerated holes and oxidizing radicals directly oxidize metals at the semiconductor/metal interface is an important process that needs to be addressed carefully. Such processes can be a major factor in determining the overall photocatalytic efficiency of metal/semiconductor nanocomposites. Efforts are underway to establish the chemical reactivity of metal nanoparticles with various oxidizing radicals using pulse radiolysis.

Since the initial formation of 480 nm absorption represents the quantitative estimate of the hole oxidation process, we monitored the formation of $(SCN)_2^{\bullet-}$ radicals at different TiO_2:Au ratios. (SinceTiO_2 is the light absorbing species, we kept the net TiO_2 core concentration constant. The TiO_2:Au ratio was varied by varying the gold concentration during sample preparation.) Figure 9 shows the dependence of $(SCN)_2^{\bullet-}$ yield on the gold concentration. The quantum yields were determined using benzophenone carboxyate (λ_{max} 535 nm, $\Phi_T = 1$) as the actinometer reference. In the absence of gold capping, TiO_2 nanoparticles generate $(SCN_2)^{\bullet-}$ radicals with a quantum yield of 0.09. Changes in $\Phi_{(SCN_2)^{\bullet-}}$ were seen as we vary the gold shell concentration. At low concentrations of gold we see an increase in the effeciency of oxidation process. For a [Au]:[TiO_2] ratio of 0.17 we see more than 40% enhancement in the oxidation efficiency ($\Phi_{(SCN_2)^{\bullet-}} = 0.13$). As we further increase the Au concentration, the efficiency of thiocyanate oxidation at gold-capped TiO_2 nanoparticles decreases. Inability of the photogenerated holes to reach the electrolyte interface and increased absorption by the gold are the likely reasons for observing lower $(SCN)_2^{\bullet-}$ yield at higher capping concentrations of gold.

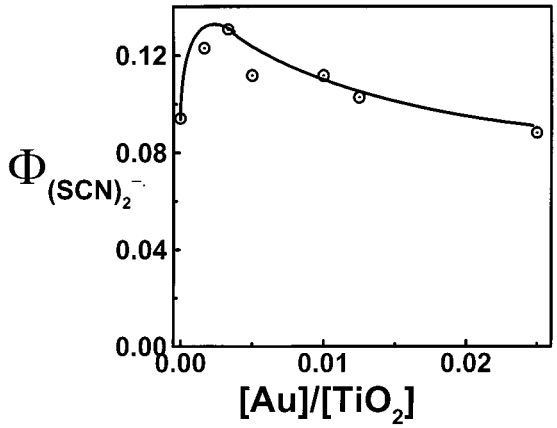

Figure 9. Dependence of $(SCN)_2^{\bullet-}$ yield on the concentration of gold cap. The maximum absorbance at 480 nm was used to determine the quantum yield of oxidation process using benzophenone carboxylate as actinometry reference.

As shown in our earlier photoelectrochemical studies,[37] deposition of gold nanoparticles on nanostructured TiO_2 films results in the enhanced photocurrent generation. Improved interfacial charge transfer at the semiconductor/electrolyte interface resulted in a nearly 3 times enhancement of photocurrent generation. When low concentrations of gold are used to cap the TiO_2 core, we can expect the outer layer to be discontinuous. Such a configuration of core/shell particles (i.e., small metal islands deposited on the TiO_2 core) provide a favorable geometry for facilitating the interfacial charge transfer under UV irradiation. Further work is underway to utilize these semiconductor/metal composite systems in immobilized films for photocatalytic applications.

Conclusions

Metal/semiconductor nanocomposites have been synthesized by the reduction of $[AuCl_4]^-$ on the surface of preformed TiO_2 nanoparticles. The concentration of the TiO_2 core directly influences the particle size and the stability of these composite nanoparticles. Aggregation effects were observed for nanoparticles with a TiO_2:Au ratio less than 1:1. Laser (532 nm) pulse excitation of these aggregated nanoparticles resulted in the fusion and formation of large multicore TiO_2 and gold shell composites. The gold-capped TiO_2 nanoparticles have been found to improve the efficiency of interfacial charge-transfer process. More than 40% enhancement in the efficiency of thiocyante oxidation was achieved using TiO_2/Au nanoparticles.

Acknowledgment. The work described herein was supported by the Office of the Basic Energy Sciences of the U.S. Department of Energy. This is contribution No. 4258 from the Notre Dame Radiation Laboratory.

References and Notes

(1) *Semiconductor Nanoclusters-Physical, Chemical and Catalytic Aspects*; Kamat, P. V., Meisel, D., Eds.; Elsevier Science: Amsterdam, 1997; p 474.
(2) Alivisatos, P. *J. Phys. Chem.* **1996**, *100*, 13226.
(3) Henglein, A. *J. Phys. Chem.* **1993**, *97*, 5457.
(4) Steigerwald, M. L.; Brus, L. E. *Acc. Chem. Res.* **1990**, *23*, 183.
(5) Link, S.; El-Sayed, M. A. *J. Phys. Chem. B* **1999**, *103*, 8410.
(6) Bechinger, C.; Ferrere, S.; Zaban, A.; Sprague, J.; Gregg, B. A. *Nature* **1996**, *383*, 608.
(7) Hagfeldt, A.; Graetzel, M. *Chem. Rev.* **1995**, *95*, 49.
(8) Klein, D. L.; Roth, R.; Lim, A. K. L.; Alivisatos, P.; McEuen, P. L. *Nature* **1997**, *389*, 699.
(9) Haesselbarth, A.; Eychmueller, A.; Eichberger, R.; Giersig, M.; Mews, A.; Weller, H. *J. Phys. Chem.* **1993**, *97*, 5333.
(10) Bedja, I.; Kamat, P. V. *J. Phys. Chem.* **1995**, *99*, 9182.
(11) Kamalov, V. F.; Little, R.; Logunov, S. L.; El-Sayed, M. A. *J. Phys. Chem.* **1996**, *100*, 6381.
(12) Mews, A.; Kadavanich, A. V.; Banin, U.; Alivisatos, A. P. *Phys. Rev.* **1996**, *B53*, R13242.
(13) Kamat, P. V. Composite Semiconductor Nanoclusters. In *Semiconductor Nanoclusters − Physical, Chemical and Catalytic Aspects*; Kamat, P. V., Meisel, D., Eds.; Elsevier Science: Amsterdam, 1997; p 237.
(14) Kraeutler, B.; Bard, A. J. *J. Am. Chem. Soc.* **1978**, *100*, 4317.
(15) Shanghavi, B.; Kamat, P. V. *J. Phys. Chem. B* **1997**, *101*, 7675.
(16) Pastoriza-Santos, I.; Koktysh, D. S.; Mamedov, A. A.; Giersig, M.; Kotov, N. A.; Liz-Marzán, L. M. *Langmuir* **2000**, *16*, 2731.
(17) Schreder, B.; Schmidt, T.; Ptatschek, V.; Winkler, U.; Materny, A.; Umbach, E.; Lerch, M.; G. Müller, G.; W. Kiefer, W.; Spanhel, L. *J. Phys. Chem. B* **2000**, *104*, 1677.
(18) Marignier, J. L.; Belloni, J.; Delcourt, M. O.; Chevalier, J. P. *Nature* **1985**, *317*, 344.
(19) Freeman, R. G.; Hommer, M. B.; Grabar, K. C.; Jackson, M. A.; Natan, M. J. *J. Phys. Chem.* **1996**, *100*, 718.
(20) Mulvaney, P.; Giersig, M.; Henglein, A. *J. Phys. Chem.* **1993**, *97*, 7061.
(21) Henglein, A. *J. Phys. Chem. B* **2000**, *104*, 6683.
(22) Lawless, D.; Kapoor, S.; Kennepohl, P.; Meisel, D.; Serpone, N. *J. Phys. Chem.* **1994**, *98*, 9619.
(23) Liz-Marzán, L. M.; Giersig, M.; Mulvaney, P. *Langmuir* **1996**, *12*, 4329.
(24) Makarova, O. V.; Ostafin, A. E.; Miyoshi, H.; Norris, J. R.; Meisel, D. *J. Phys. Chem. B* **1999**, *103*, 9080.
(25) Hardikar, V.; Matijevic, E. *J. Colloid Interface Sci* **2000**, *221*, 133.
(26) Kamat, P. V. *Chem. Rev.* **1993**, *93*, 267.
(27) Bard, A. J. *J. Phys. Chem.* **1982**, *86*, 172.
(28) Bard, A. J.; Fox, M. A. *Acc. Chem. Res.* **1995**, *28*, 141.
(29) Nosaka, Y.; Norimatsu, K.; Miyama, H. *Chem. Phys. Lett.* **1984**, *106*, 128.
(30) Nasr, C.; Hotchandani, S.; Kim, W. Y.; Schmehl, R. H.; Kamat, P. V. *J. Phys. Chem. B* **1997**, *101*, 7480.
(31) Nasr, C.; Hotchandani, S.; Kamat, P. V. *J. Phys. Chem. B* **1998**, *102*, 10047.
(32) Vinodgopal, K.; Kamat, P. V. *Environ. Sci. Technol.* **1995**, *29*, 841.
(33) Tada, H.; Teranishi, T. K.; Yo-ichi, I.; Ito, S. *Langmuir* **2000**, *16*, 3304.
(34) de Tacconi, N. R.; Carmona, J.; Rajeshwar, K. *J. Phys. Chem. B* **1997**, *101*, 10151.
(35) Chen, S. H.; Kimura, K. *Chem. Lett.* **1999**, 233.
(36) Vijaya Sarathy, K.; John Thomas, P.; Kulkarni, G. U.; Rao, C. N. R. *J. Phys. Chem. B* **1999**, *103*, 399.
(37) Chandrasekharan, N.; Kamat, P. V. *J. Phys. Chem. B* **2000**, *104*, 10851.
(38) Averitt, R. D.; Westcott, S. L.; Halas, N. J. *J. Opt. Soc. Am. B. Opt. Phys.* **1999**, *16*, 1814.
(39) Averitt, R. D.; Westcott, S. L.; Halas, N. J. *J. Opt. Soc. Am. B. Opt. Phys.* **1999**, *16*, 1824.
(40) Oldenburg, S. J.; Jackson, J. B.; Westcott, S. L.; Halas, N. J. *Appl. Phys. Lett.* **1999**, *75*, 2897.
(41) Westcott, S. L.; Oldenburg, S. J.; Lee, T. R.; Halas, N. J. *Chem. Phys. Lett.* **1999**, *300*, 651.
(42) Kamat, P. V.; Ebbesen, T. W.; Dimitrijevic, N. M.; Nozik, A. J. *Chem. Phys. Lett.* **1989**, *157*, 384.
(43) Ocana, M.; Hsu, W. P.; Matijevic, E. *Langmuir* **1991**, *7*, 2911.
(44) Giesche, H.; Matijevic, E. *J. Mater. Res.* **1994**, *9*, 436.
(45) Averitt, R. D.; Westcott, S. L.; Oldenburg, S. J.; Lee, T. R.; Halas, N. J. *Langmuir* **1998**, *14*, 5396.
(46) Kamat, P. V.; Flumiani, M.; Hartland, G. *J. Phys. Chem. B* **1998**, *102*, 3123.
(47) Fujiwara, H.; Yanagida, S.; Kamat, P. V. *J. Phys. Chem. B* **1999**, *103*, 2589.
(48) Takami, A.; Kurita, H.; Koda, S. *J. Phys. Chem. B* **1999**, *103*, 1226.
(49) Link, S.; Burda, C.; Mohamed, M. B.; Nikoobakht, B.; El-Sayed, M. A. *J. Phys. Chem. A* **1999**, *103*, 1165.
(50) Heilweil, E. J.; Hochstrasser, R. M. *J. Chem. Phys.* **1985**, *82*, 179.
(51) Ahmadi, T. S.; Logunov, S. L.; El-Sayed, M. A. *J. Phys. Chem.* **1996**, *100*, 8053.
(52) Link, S.; Burda, C.; Nikoobakht, B.; El-Sayed, M. A. *Chem. Phys. Lett.* **1999**, *315*, 12.
(53) Heller, A. *Pure Appl. Chem.* **1986**, *58*, 1189.
(54) Nosaka, Y.; Ishizuka, Y.; Miyama, H. *Ber. Bunsen-Ges. Phys. Chem.* **1986**, *90*, 1199.
(55) Chen, Y.; Wei, Z.; Chen, Y.; Lin, H.; Hong, Z.; Liu, H.; Dong, Y.; Yu, C.; Li, W. *J. Mol. Catal.* **1983**, *21*, 275.
(56) Nakato, Y.; Tsubomura, H. *Isr. J. Chem.* **1982**, *22*, 180.
(57) Kamat, P. V. *Langmuir* **1985**, *1*, 608.
(58) Behar, D.; Bevan, P. L. T.; Scholes, G. *J. Phys. Chem.* **1972**, *76*, 1537.
(59) Dawson, A.; Kamat, P. V. *J. Phys. Chem. B* **2000**, *104*, 11842.